Integrated decouple inductance winding planar transformer for LLC converter

Dinh-Duc Quach[1], Quang-Huy Nguyen[1], Khuong-Duy Le[1] and Duy-Dinh Nguyen[1,*]

[1]*Hanoi University of Science and Technology, Hanoi, Vietnam*
[*]*Corresponding author E-mail: dinh.nguyenduy@hust.edu.vn*
DOI: https://doi.org/10.64032/mca.v29i4.340

Abstract

The increasing demand for high power density and efficiency in DC-DC converters is proposed the LLC resonant converter as a promising topology for applications such as photovoltaic systems, DC power distribution, and electric vehicle charging. The transformer in LLC converters significantly influences power density, cost, and efficiency, making magnetic design optimization critical. While planar transformers offer advantages like low profile, improved thermal performance, and high power density compared to traditional wire-wound transformers, discrete magnetic components increase system volume, weight, and losses. Magnetic integration, particularly utilizing transformer leakage inductance as a resonant inductor, is a compelling solution to enhance compactness and efficiency. However, existing integration methods face challenges, including insufficient leakage inductance, high core losses, and complex core designs. This paper proposes a novel magnetically integrated LLC resonant converter with decoupled inductor windings that amalgamates resonant and magnetizing inductance within a unified core using a split-integration magnetic flux approach. A detailed analysis of magnetic flux dynamics yields optimized design equations, validated through finite element modeling of flux density and field distribution. Experimental results at 250 kHz resonant frequency and 180 W output power demonstrate the superiority of the proposed design over traditional separate transformers and prior integrated structures with asymmetric windings, achieving improved power density, reduced losses and simplified design procedure.

Keywords: *LLC resonant converter; Planar transformer; PCB winding; Integrated transformer and decouple inductance winding.*

Abbreviations

L_{lk}	Leakage inductance
L_m	Magnetizing inductance

1. Introduction

With the progressive evolution of power electronics technology, the importance of high-power density and high-efficiency DC-DC converters has increasingly been shown in various industrial applications, including photovoltaic (PV) generation systems [1], DC power distribution networks [2], and electric vehicle charging systems [3], [4]. An example of such an EV charging system is depicted in Fig. 1. The LLC resonant converter is a promising topology for these applications not only because of the ability to provide galvanic isolations for distributed power sources, but also greatly improve the system efficiency due to the zero-voltage soft-switching (ZVS) capability [5], [6].

For the LLC converter, the transformer plays a crucial role, influencing power density, manufacturing cost, and overall system efficiency [7]. Thus, optimizing the magnetic design is essential to enhance the converter's performance. Today, two common magnetic circuit structures utilized in both research and industrial applications are conventional wire-wound transformers and planar transformers. Planar transformers have gained significant traction in high-frequency power conversion applications, particularly LLC converters, owing to their compact form factor, efficient heat dissipation, modular architecture, ease of fabrication, enhanced operational reliability, and higher power density [8], [9]. In contrast, traditional wire-wound transformers have revealed limitations in these requirements. Therefore, the planar magnetic option will be preferred for high-performance applications.

In conventional LLC converter configurations, planar magnetics are often implemented using separate components namely a planar transformer and an individual planar resonant inductor. Nonetheless, the use of distinct magnetic elements tends to increase the system's overall size, weight, manufacturing cost, and power losses [10], thereby adversely affecting the converter's efficiency and power density. To overcome these limitations, integrating magnetic components has emerged as a favorable approach. One effective method is to leverage the inherent leakage inductance of the transformer to replace the discrete resonant inductor, enabling a more compact and efficient converter design [11], [12].

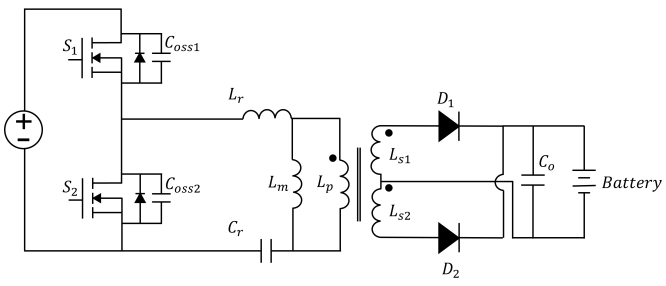

Figure 1: Topology of LLC converter in EV charging application.

Received: 14 May 2025; Revised: 16 July 2025; Accepted: 19 August 2025.

There are many methods of integrating magnetic components that have been researched and applied to LLC converters [11], [12], [13], [14]. Among these, utilizing the transformer's leakage inductance to fulfill the role of a resonant inductor is a commonly favored approach to reduce both component count and converter volume [11], [12]. In [11], the authors introduced a design approach where the primary and secondary windings are physically separated to effectively regulate the leakage inductance. But this integrated transformer is often unsuitable for PCB winding transformers because of the limited leakage inductance generated by this method is not enough to achieve the required resonant inductance. To solve this problem, [12] introduces the use of a magnetic shunt made from low permeability material, creating an auxiliary flux path that intentionally enhances the transformer's leakage inductance. Nonetheless, the use of low-permeability materials in magnetic shunt structures, as proposed in [12], typically results in significant core losses, which adversely affect the transformer's overall efficiency. In addition, incorporating such shunts enlarges the magnetic core, thereby increasing the physical size and manufacturing cost. In the approaches outlined in [11] and [12], where air is employed as the main energy storage medium, the increased magnetomotive force (MMF) across the windings leads to higher AC losses in the copper conductors, ultimately degrading system performance. An alternative technique introduced in [13] combines both the transformer and resonant inductor within a unified magnetic core. This design involves merging one of the transformer windings, either primary or secondary, with the winding of a series inductor. While this approach reduces component count, it requires specially shaped cores that are not standard in the commercial market, thus limiting its practicality. In [14], another strategy is proposed using a custom core where the PCB windings for primary and secondary are placed asymmetrically on the outer legs, allowing the leakage flux to concentrate through the central leg and achieve the desired leakage inductance. Although this semi-interleaved configuration provides benefits such as reduced AC resistance and the ability to fine-tune leakage inductance, it also introduces considerable complexity in both winding layout and core structure. Additionally, wrapping the windings around the outer legs contributes to a bulkier transformer and increased magnetic core losses.

In summary, although existing magnetic integration techniques have contributed to reduced component count and enhanced power density in LLC resonant converters, challenges related to precise leakage inductance control and loss minimization persist. To overcome these issues, this work introduces a novel magnetically integrated LLC converter that features decoupled inductor windings within a unified core structure. The proposed design adopts a split-flux integration strategy to combine both resonant and magnetizing inductance effectively into the transformer core. A comprehensive magnetic flux analysis was carried out, resulting in the formulation of design-optimized equations. ANSYS Maxwell 2D-transient simulations were employed to verify the magnetic field and flux density distribution across critical components. An experimental prototype operating at a 250 kHz resonant frequency and delivering 180 W of output power was constructed. The developed converter achieves a 26.68% reduction in physical size, a 10% decrease in transformer losses, and reaches a peak efficiency of 93%.

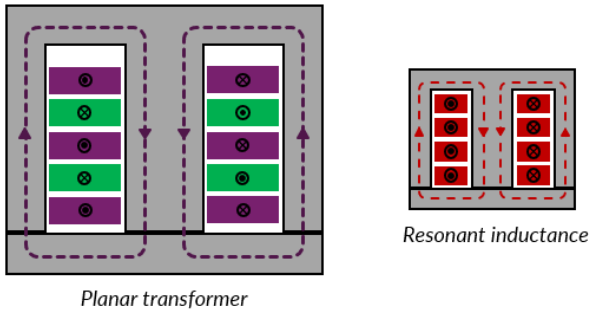

Figure 2: The traditional separate planar transformer and resonant inductor.

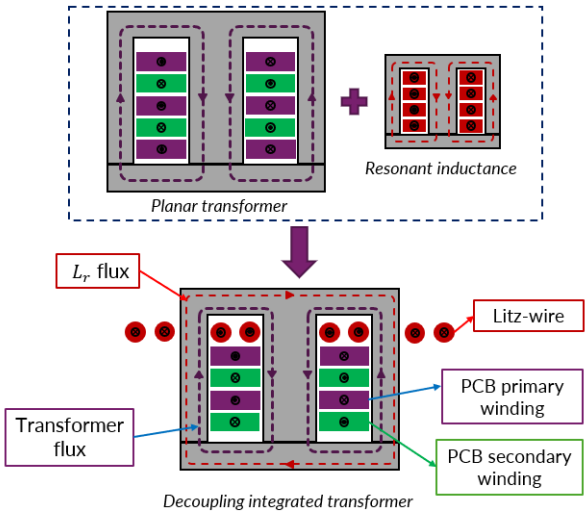

Figure 3: The proposed decouple integrated transformer.

2. Planar magnetic integration method

2.1. Traditional discrete planar magnetic

In conventional LLC converter implementations, the layout of discrete planar magnetic components is typically illustrated as in Fig. 2. This structure is composed of three individually defined magnetic elements, namely the resonant inductance (L_r), the magnetizing inductance (L_m), and the planar transformer. The resonant inductance is usually realized through a standalone planar inductor designed to meet specific inductance requirements, while the magnetizing inductance is incorporated by introducing an air gap in the planar transformer core. Furthermore, interleaving the primary and secondary windings on the PCB is a widely adopted method in planar transformer design, as it effectively minimizes high-frequency AC winding losses [15], [16].

However, this conventional design presents several limitations. In particular, the planar resonant inductor, an essential component within the magnetic assembly, often becomes a constraint in efforts to minimize size, cost, and energy losses in both the magnetic subsystem and the general converter [12]. To address this issue, an increasingly favored approach involves exploiting the transformer's inherent leakage inductance to fulfill the role of the resonant inductor, thereby reducing the total number of magnetic elements and enabling a more compact converter design.

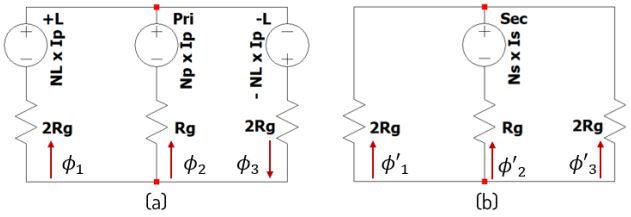

Figure 4: Reluctance model (a) open-circuited secondary side (b) open-circuited primary side.

2.2. Propose decoupling integrated planar transformer

Magnetic integration offers an effective solution to system simplification by allowing the transformer's leakage inductance to fulfill the role of external inductors. However, achieving the appropriate leakage inductance level is essential for meeting the converter's design specifications. Fig. 3 presents the structural design of the integrated transformer introduced in this research. Building on the benefits of planar magnetics discussed previously such as compact size, high power density, reduced AC losses in windings, and the potential to embed magnetizing inductance—the basic structure of a traditional planar transformer is preserved in the proposed design. The PCB windings are fully interleaved on the central limb of the magnetic core, ensuring efficient coupling between primary and secondary sides. To effectively utilize the available core area, the resonant inductor litz windings are arranged on the outer limbs of the core. An identical air gap is introduced on all three limbs to facilitate proper magnetic behavior. As shown in Fig. 3, the flux paths generated by the transformer and resonant windings are spatially separated, ensuring minimal magnetic coupling. This structural decoupling confirms the presence of intrinsic leakage inductance in the integrated configuration. Furthermore, the leakage inductance can be precisely controlled by adjusting the air gaps on the outer legs, making the design adaptable to different application needs. Meanwhile, the magnetizing inductance remains regulated through the air gap in the central leg, maintaining functional separation between the two inductive elements.

3. Analysis of reluctance model of proposed integrated transformer

Based on the transformer topology in Fig. 3, a magnetic reluctance model is built, as shown in Fig. 4 (a) and Fig. 4 (b). In this context, Fig. 4 (a) illustrates the equivalent magnetic circuit of the proposed transformer when the secondary side is open circuit, while Fig. 4 (b) represents the equivalent magnetic circuit when the primary side is open-circuit. In this model, N_p and N_s denote the number of turns on the primary and secondary transformer windings, respectively. The turns of the integrated resonant inductance windings placed on the outer limbs are represented by N_L. The currents flowing through the primary and secondary windings are designated as I_P and I_S. The resulting magnetic fluxes in the three core limbs are represented as ϕ_1, ϕ_2 and ϕ_3, corresponding to the flux paths induced by the interaction of the windings and magnetic core columns. To simplify the analysis without sacrificing precision, two assumptions are introduced: the magnetic permeability of the core material is considered much higher than that of air, which is approximated to unity and leakage flux in the surrounding air is minimal and therefore neglected. To facilitate design while preserving the structural integrity of the magnetic core, identical air gaps l_g are introduced simultaneously in all three legs of the core. Let A, A_1 and A_2 represent the cross-sectional areas of the outer and center legs, respectively. Given that an EE-type magnetic core is employed, the relationship among these areas is defined as $A = 2A_1 = 2A_2$. Consequently, the total magnetic reluctance is primarily determined by the open air gaps within the magnetic path:

$$R_g = \frac{l_g}{\mu A},\ R_g1 = \frac{l_g1}{\mu A1},\ R_g2 = \frac{l_g2}{\mu A2} \tag{1}$$

with $\mu = 4\pi 10^{-7}$ is the air permeability. As a result, the reluctance introduced by the air gaps in the outer legs and the center leg of the magnetic core are denoted in Fig. 4 as $2R_g$ and R_g. Based on the reluctance model under secondary-side open-circuit conditions, the magnetic flux in each limb of the core, as illustrated in Fig. 4(a), can be determined using the following expressions:

$$\phi_1 = \frac{2 \times N_L \times I_P - N_P \times I_P}{4 \times R_g} \tag{2}$$

$$\phi_2 = \frac{N_P \times I_P}{2 \times R_g} \tag{3}$$

$$\phi_3 = \frac{2 \times NL \times I_P + N_P \times I_p}{4 \times R_g} \tag{4}$$

Similarly, based on the reluctance model when the primary side of the transformer is open-circuited, as shown in Fig. 4 (b), the magnetic fluxes in the core limbs are expressed as follows:

$$\phi'_1 = \phi'_3 = \frac{N_S \times I_S}{4 \times R_g} \tag{5}$$

$$\phi'_2 = \frac{N_S \times I_S}{2 \times R_g} \tag{6}$$

From equations (2) to (6), it can be observed that ϕ_2 and ϕ'_2 are completely independent of the integrated resonant inductance component (N_L). Therefore, the magnetizing inductance on the primary and secondary sides can be determined as:

$$L_{m,p} = \frac{N_P \times \phi_2|_{i_S=0}}{I_P} = \frac{N_P^2}{2 \times R_g} \tag{7}$$

$$L_{m,s} = \frac{N_s \times \phi'_2|_{i_p=0}}{I_s} = \frac{N_s^2}{2 \times R_g} \tag{8}$$

Together with (3) and (6), we can calculate the resonant inductance by following equations:

$$L_{lk} = \frac{N_L \times \phi}{I_p} = \frac{\mu_r \times \mu_0 \times A_C \times N_L^2}{MPL} = \frac{N_L^2}{4 \times R_g} \tag{9}$$

- μ: magnetic core permeability, MPL: magnetic path length

The proposed configuration of the core transformer allows independent adjustment of magnetizing inductance (L_m) and

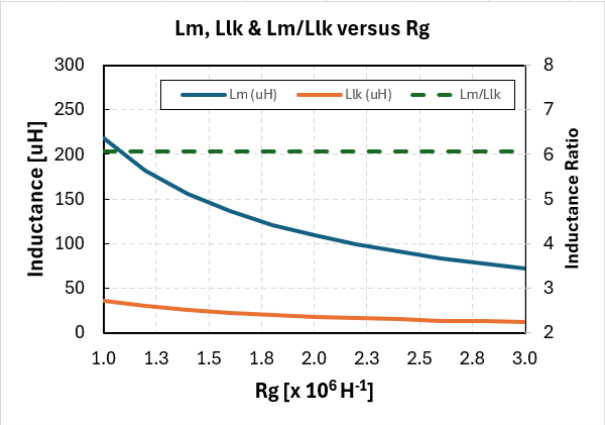

Figure 5: Survey of inductance under R_g variations and constant N_L.

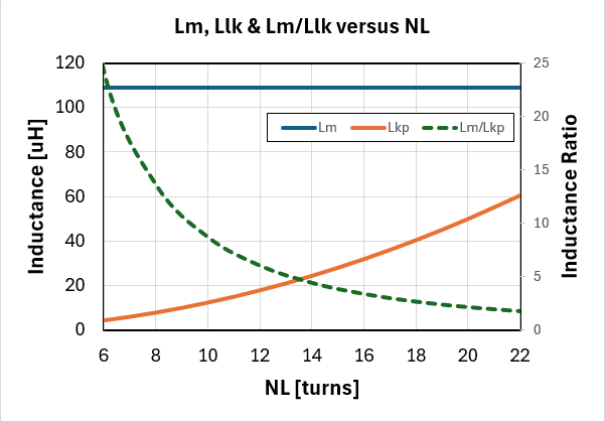

Figure 6: Survey of inductance under N_L variations and constant R_g.

leakage inductance (L_{lk}) by using different combinations of air gap resistance R_g. Due to the spatial separation, the flux associated with the resonant inductors on both sides of the core does not interfere with the central transformer core, and vice versa. This mutual independence of magnetic flux paths ensures that the transformer and resonant inductance operate without magnetic coupling. Therefore, a comprehensive analysis of the proposed integrated transformer model has been completed and it is shown that the transformer can be designed for most reasonable specifications in terms of leakage and magnetizing inductance.

From equations (7),(8) and (9), Fig. 5 and 6 illustrate the variation of magnetizing and leakage inductance while maintaining a constant integrated resonant winding distribution ($N_L = 12$ turns) and air gap reluctance ($R_g = 2e6\ H^{-1}$). It is evident that both the air gap reluctance R_g and the number of turns in the integrated resonant winding N_L serve as key reference parameters in identifying the dominant design-influencing factors.

4. Proposed integrated planar transformer design procedure

The integrated transformer design procedure, illustrated in Fig. 7, comprises the following steps: First, design parameters are selected as the foundation for determining a suitable magnetic core. Subsequently, the winding structure is designed to satisfy the required inductance values. Finally, the complete

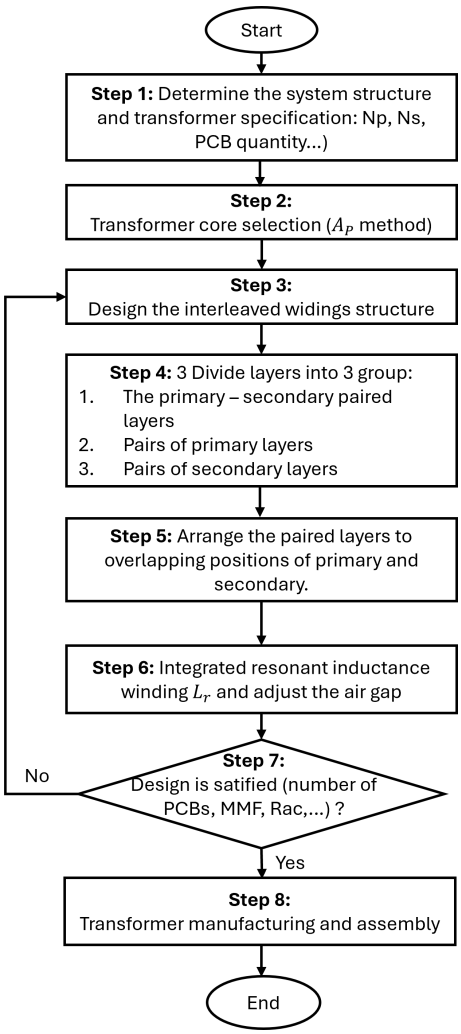

Figure 7: Design procedure of proposed transformer.

PCB layer 1.6mm		
PCB1	Coating	0.02
	Layer 1	0.07
	FR4	0.1835
	Layer 2	0.061
	FR4	0.96
	Layer 3	0.061
	FR4	0.1835
	Layer 4	0.07
	Coating	0.02
Isolated	Paper	0.0476
PCBn		

Figure 8: Four-layer PCB windings.

design is verified and evaluated to ensure compliance with the initial specifications. The details of the implementation steps will be presented in the following.

In step 1, the design requirements for the transformer are defined. The turns ratio is specified as $N_p : N_{s1} : N_{s2} = 20 : 6 : 6$, and a four-layer PCB is selected with its structural layout shown in Fig. 8.

The method of calculating the core size is based on the parameter A_p in Step 2. Thereby, it is easy to choose the PQ32/20 core made of N87 material with parameters suitable for the design requirements.

In the step 3, interleaving between the primary and secondary PCB windings is applied in accordance with the MMF

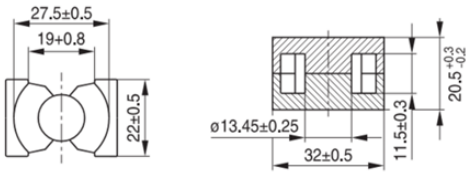

Figure 9: PQ32/20 core structure and parameters.

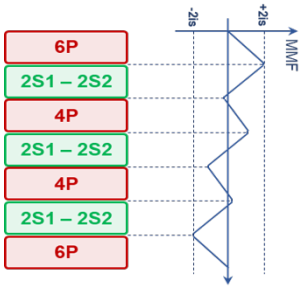

Figure 10: Interleaved winding structure.

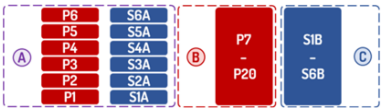

Figure 11: Paired layer group and non-paired layer groups.

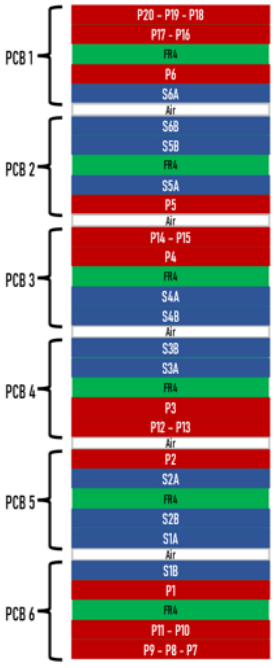

Figure 12: Arrange the PCB layers.

distribution strategy, aiming to minimize high-frequency AC losses in the windings.

Fig. 11 and 12 represent steps 4 and 5, and the PCB layers are categorized into laminated and non-laminated groups to facilitate the layer arrangement according to the proposed winding structure.

The Litz-winding is wound around the two outer pillars of the magnetic core to adjust the leakage inductance to achieve the required resonant inductance in step 6 is shown in Fig. 13.

Finally, steps 7 and 8 involves designing the PCB layout

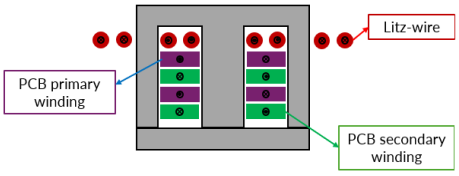

Figure 13: Integrated litz-windings on outer core leg.

Table 1: Implemented LLC converter's specification

Parameter	Value
$N_P : N_{S1} : N_{S2}$	20:6:6
L_m	110 μ H
L_r	20.5 μ H
C_r	19.8 nF
V_{in}	230 VAC
V_{out}	46 - 60 V
I_{out}	3 A
P_{out}	138 - 180 W
f_s	175 - 300 kHz

and verifying the transformer assembly to ensure the requirements of inductance and minimize the transformer losses.

5. Simulation of proposed integrated magnetic

A planar transformer is developed using the formulas outlined in Section 3. The magnetizing inductance, leakage inductance, and winding ratio of the transformer are selected to meet the requirements of a sample isolated LLC resonant converter, as specified in Table 1. To verify the theoretical analysis, the results ANSYS Maxwell 2D-transient electromagnetic simulation of the designed transformer are presented below.

The complete flux distribution through three leg on magnetic core over switching cycles is demonstrated in Fig. 14. It can be seen that the proposed transformer flux waveform at the right outer pillar (ϕ_3) has a very large deviation from the flux passing through the other two pillars (ϕ_1 and ϕ_2) of the magnetic core.

In the proposed planar transformer design, the leakage inductance is utilized to serve as the resonant inductance. The primary and secondary windings are arranged vertically along the magnetic core. Fig. 15 illustrates a finite element analysis of the transformer, showing a peak magnetic flux density of approximately 0.44 T at the outer leg of the core. The magnetic flux in this design arises from both the resonant inductance winding and the primary winding, distributing evenly across the central and lateral columns. A small amount of fringe flux is observed at the air gaps of the side columns, leading to negligible magnetic leakage. This configuration effectively minimizes the coupling between the magnetic fluxes.

Table 2 presents the simulation results for both transformers. The results for the standalone transformer closely align with those for the integrated transformer, confirming the reliability of the system. Additionally, the magnetic flux density within the core is distributed evenly, with no instances of significant localized flux concentration. Throughout the operational cycle, the core remains below its saturation flux density, demonstrating that the chosen core for the integrated transformer meets the design specifications outlined in this research.

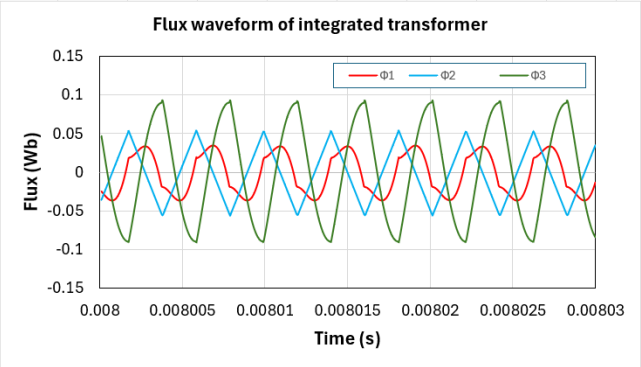

Figure 14: Flux waveform of the integrated transformer.

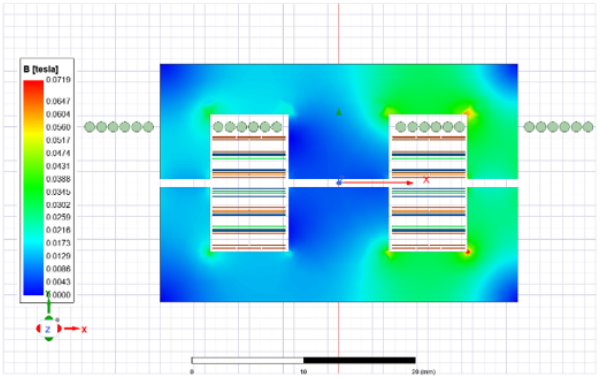

Figure 15: Magnetic flux density distribution of integrated transformer.

Table 2: Simulation results of separate and integrated magnetic

Parameter	Separate magnetic	Integrated magnetic
L_{lk}	21.1 μH	20.5 μH
L_m	108.71 μH	110.18 μH

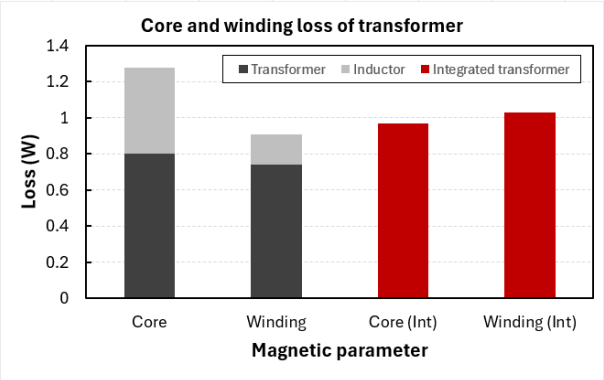

Figure 16: Comparison between the proposed transformer and the standard transformer + inductor at the same output power 180 W.

The enhancements proposed in this study enable a more effective integration of the transformer and inductor compared to the traditional method of designing a conventional transformer alongside a separate inductor. Fig. 16 illustrates a loss comparison between the integrated transformer and the standard transformer with a standalone inductor, highlighting the improved efficiency of the proposed design. This comparison is performed under identical conditions, using the same magnetic footprint and output power for both configurations.

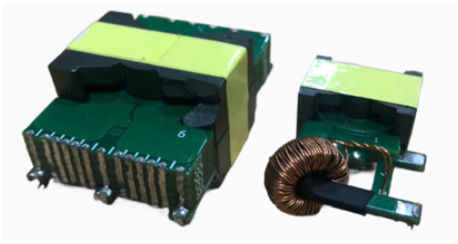

Figure 17: Prototypes of the discrete transformer.

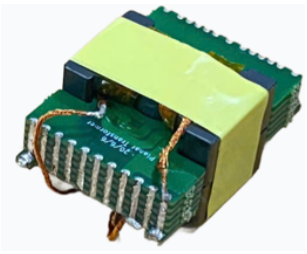

Figure 18: Prototypes of the integrated transformer.

Table 3: Experimental results of separate and integrated magnetic

Parameter	Separate magnetic	Integrated magnetic
L_{lk}	23.6 μH	22.2 μH
L_m	118.3 μH	115.5 μH

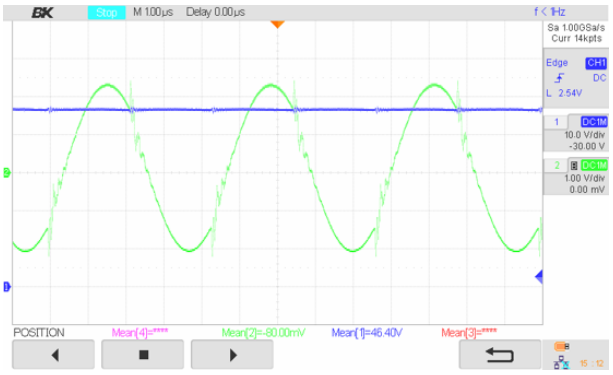

Figure 19: The resonant current of LLC converter using discrete magnetic on 46 V output voltage.

6. Experimental results

To verify theoretical analysis and simulation results, an integrated magnetic based on the proposed structure with specifications given in Table 1 is built and shown in Fig. 18. For comparison, a separate resonant inductor and transformer are also built to the same specification, shown in Fig. 17.

The measured leakage and magnetizing inductance of the proposed topology at 250 kHz obtained using an LCR GW INSTEK LCR-916 are given in Table 3. According to Table 3, the leakage and magnetizing inductance obtained by ANSYS Maxwell 2D-transient electromagnetic simulation and modeling are close to the experimental results.

Fig. 19 shows the experiment resonant current waveforms of LLC resonant converter with discrete transformer and Fig. 20 shows the experimental resonant current waveforms of LLC resonant converter with integrated transformer. The resonant current of the converter when using separate and integrated transformer structures has relatively similar waveforms. It can

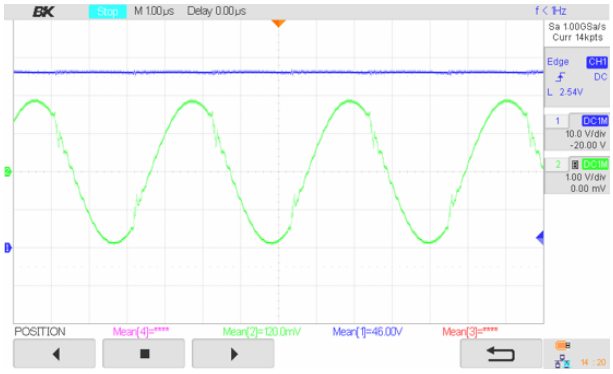

Figure 20: The resonant current of LLC converter using integrated magnetic on 46 V output voltage.

be seen that the converter operates correctly with both transformer. Furthermore, CM noise oscillation exists on the waveform due to the influence of parasitic capacitors or measuring devices during the experiment.

Through measurement under the constant switching frequency of 250 kHz, compared with separate transformer, the volume and weight of integrated transformer are reduced by 26.68%, which increases the power density of the converter.

Fig. 21 illustrates the efficiency of the LLC converter across various load conditions, comparing the proposed integrated transformer with the conventional discrete transformer. From this observation, it is evident that the converter employing the proposed integrated planar transformer structure achieves higher efficiency compared to the conventional design with a separate inductor. This result demonstrates that the integrated transformer has been effectively designed to fulfill the efficiency requirements of the system. The proposed design achieves 93% peak efficiency compared to 92.16% using the conventional structure. Furthermore, Fig. 22 shows the thermal performance tested under full load (180 W) after steady-state thermal is reached with no heat sink. As shown, the proposed topology operates at a low temperature (35.7°C). In addition, the temperature of the outer core leg of one side is higher than in the other core's parts, verifying the magnetic flux density distribution in Fig. 15.

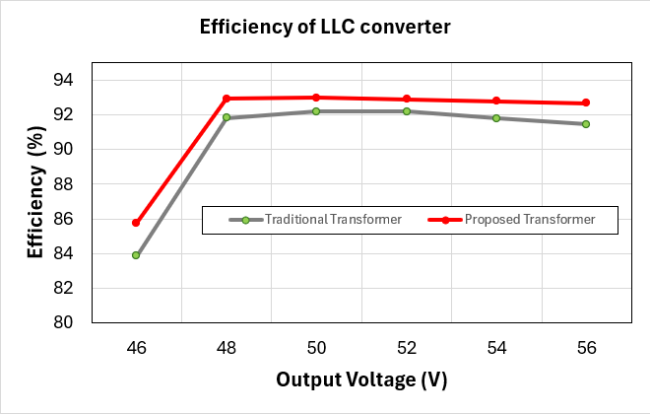

Figure 21: Efficiency curve over full output voltage range.

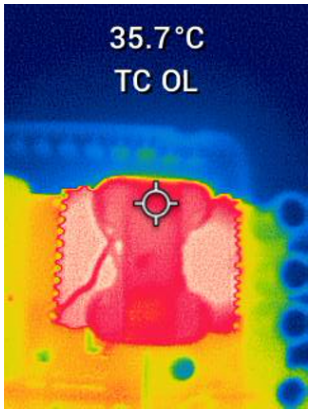

Figure 22: Thermal image of the proposed transformer.

7. Conclusion

In this paper, a magnetically integrated LLC resonant converter with independent inductance windings is proposed. By employing a decoupled integration method, the resonant and magnetizing inductance are effectively integrated with the transformer within a single magnetic core. This integration ensures that the resonant inductor and transformer operate independently without mutual interference, thereby enabling the converter to achieve stable and high-efficiency performance. Compared to existing magnetic integration solutions for LLC resonant converters, the proposed method effectively reduces the leakage inductance between transformer windings and mitigates magnetic saturation in the integrated core. As a result, core losses are minimized and the overall efficiency of the converter is significantly improved. A hardware prototype with 93 % efficiency is built and the experimental result verifies the proposed concept.

Acknowledgement

This work is funded by Hanoi University of Science and Technology (HUST) under Project T2023-TD-008.

References

[1] M. Wang et al., "Module power balance control strategy for three-phase cascaded H-Bridge PV inverter under unbalanced grid voltage condition," IEEE J. Emerg. Sel. Topics Power Electron., vol. 9, no. 5, pp. 5657–5671, Oct. 2021.

[2] D. Sha, J. Zhang, and K. Liu, "Leakage inductor current peak optimization for dual-transformer current-fed dual active bridge DC–DC converter with wide input and output voltage range," IEEE Trans. Power Electron., vol. 35, no. 6, pp. 6012–6024, Jun. 2020, doi: 10.1109/TPEL.2019.2952650.

[3] H. Wang and Z. Li, "A PWM LLC type resonant converter adapted to wide output range in PEV charging applications," IEEE Trans. Power Electron., vol. 33, no. 5, pp. 3791–3801, May 2018.

[4] Z. Li, T. Wu, G. Zhang, and R. Yang, "Hybrid modulation method combining variable frequency and double phase-shift for a 10 kW LLC resonant converter," IET Power Electron., vol. 11, no. 13, pp. 2161–2169, Jul. 2018.

[5] Y. Gu, Z. Lu, L. Hang, Z. Qian, and G. Huang, "Three-level LLC series resonant DC/DC converter," IEEE Trans. Power Electron., vol. 20, no. 4, pp. 781–789, Jul. 2005.

[6] S. De Simone, C. Adragna, C. Spini, and G. Gattavari, "Design-oriented steady-state analysis of LLC resonant converters based on FHA," in Proc. Int. Symp. Power Electron., Elect. Drives Autom. Motion, 2006, pp. 200–207.

[7] Y. Wei, Q. Luo and H. A. Mantooth, "An LLC Converter With Multiple Operation Modes for Wide Voltage Gain Range Application," in IEEE Transactions on Industrial Electronics, vol. 68, no. 11, Nov.2021.

[8] Z. Li, X. Yang, Y. Li, J. Li, B. Zhang and T. Lei, "Design and Implementation of a High-efficiency DC/DC Converter for EVs Charging Basing on LLC Resonant Topology and Silicon-Carbide Devices," 2018

IEEE International Power Electronics and Application Conference and Exposition (PEAC), Shenzhen, China, 2018.
[9] Z. Lu and W. Chen, “Research on magnetic integration technology of multi-channel interleaved parallel flyback converter,” Proc. CSEE, vol. 29, no. 18, pp. 41–46, 2009.
[10] [11] Q. Chen, X. Ruan, and Y. Yan, “Magnetic integration technology and its application in switching power supply,” Trans. China Electrotech. Soc., vol. 19, no. 3, pp. 1–8, 2004.
[11] M. Li, Q. Chen, X. Ren, Y. Zhang, K. Jin and B. Chen, "The integrated LLC resonant converter using center-tapped transformer for on-board EV charger," 2015 IEEE Energy Conversion Congress and Exposition (ECCE), Montreal, QC, Canada, 2015.
[12] S. A. Ansari, J. N. Davidson and M. P. Foster, "Inserted-Shunt Integrated Planar Transformer With Low Secondary Leakage Inductance for LLC Resonant Converters," in IEEE Transactions on Industrial Electronics, vol. 70, no. 3, pp. 2652-2661, March 2023.
[13] Y. Liu, H. Wu, J. Zou, Y. Tai and Z. Ge, "CLL Resonant Converter With Secondary Side Resonant Inductor and Integrated Magnetics," in IEEE Transactions on Power Electronics, vol. 36, no. 10, pp. 11316-11325, Oct. 2021, doi: 10.1109/TPEL.2021.3074646.
[14] B. Li, Q. Li and F. C. Lee, "High-Frequency PCB Winding Transformer With Integrated Inductors for a Bi-Directional Resonant Converter," in IEEE Transactions on Power Electronics, vol. 34, no. 7, pp. 6123-6135, July 2019, doi: 10.1109/TPEL.2018.2874806.
[15] M. A. Saket, M. Ordonez, M. Craciun and C. Botting, "Improving Planar Transformers for LLC Resonant Converters: Paired Layers Interleaving," in IEEE Transactions on Power Electronics, vol. 34, no. 12, pp. 11813-11832, Dec. 2019, doi: 10.1109/TPEL.2019.2903168.
[16] R. Yu, T. Chen, P. Liu and A. Q. Huang, "A 3-D Winding Structure for Planar Transformers and Its Applications to LLC Resonant Converters," in IEEE Journal of Emerging and Selected Topics in Power Electronics, vol. 9, no. 5, pp. 6232-6247, Oct. 2021, doi: 10.1109/JESTPE.2021.3052712.